Journal of Biomedical Optics

BiomedicalOptics.SPIEDigitalLibrary.org

Coexpression of CdSe and CdSe/CdS quantum dots in live cells using molecular hyperspectral imaging technology

Qingli Li
Hui Peng
Jing Wang
Yiting Wang
Fangmin Guo

SPIE.

Coexpression of CdSe and CdSe/CdS quantum dots in live cells using molecular hyperspectral imaging technology

Qingli Li,[a,*] Hui Peng,[a] Jing Wang,[b] Yiting Wang,[b] and Fangmin Guo[a]
[a]East China Normal University, Shanghai Key Laboratory of Multidimensional Information Processing, No. 500, Dongchuan Road, Shanghai 200241, China
[b]East China Normal University, Institutes for Advanced Interdisciplinary Research, No. 3663, Zhoangshan Road (N), Shanghai 200062, China

Abstract. A direct spatial and spectral observation of CdSe and CdSe/CdS quantum dots (QDs) as probes in live cells is performed by using a custom molecular hyperspectral imaging (MHI) system. Water-soluble CdSe and CdSe/CdS QDs are synthesized in aqueous solution under the assistance of high-intensity ultrasonic irradiation and incubated with colon cancer cells for bioimaging. Unlike the traditional fluorescence microscopy methods, MHI technology can identify QD probes according to their spectral signatures and generate coexpression and stain titer maps by a clustering method. The experimental results show that the MHI method has potential to unmix biomarkers by their spectral information, which opens up a pathway of optical multiplexing with many different QD probes. [DOI: 10.1117/1.JBO.20.11.110504]

Keywords: spectral imaging; quantum dots; image detection systems; medical and biological imaging.

Paper 150170LRRR received Mar. 16, 2015; accepted for publication Oct. 20, 2015; published online Nov. 20, 2015.

In the past two decades, quantum dots (QDs) have attracted major interest as fluorophores in fields ranging from electronic materials science to biomedical research. They are typically produced from luminescent semiconductors, carbon and silicon nanoparticles with several unique properties: wide excitation spectra and narrow, symmetrical emission spectra, photostability, and the ability to be conjugated to a wide range of biological targets.[1] These unique properties of QDs can be finely tuned by varying their size, shape, composition, and mean interparticle distance. These properties render them near-perfect fluorescent biomarkers and superior to traditional organic fluorophores and antibodies. Most QDs are near-spherical semiconductor nanocrystals composed of a CdSe, CdS, or CdTe core combined with a ZnS shell. Their size-tunable photoluminescence is distributed throughout the visible region of the electromagnetic spectrum, making them good substitutes for organic dye molecules.[2] These QDs have been increasingly utilized in biosensors,[1] drug delivery,[3] and biological imaging.[4] In recent years, a number of research efforts have been carried out to use QDs as biomarkers for molecular and cellular imaging,[5] fluorescence imaging,[6] and targeted cancer imaging.[7] Most of these studies use fluorescence microscopy as the primary tool for evaluating the probe properties of QDs and observing the biological targets. With the improved resolution, sensitivity, and versatility of fluorescence microscopy, QD labeling in cells yields a clear understanding of the dynamics of intracellular networks, signal transduction, and cell-to-cell interaction in the fields such as immunophenotyping and clinical cytogenetics. However, there are still problems associated with the use of QDs in fluorescence microscopy for biological imaging. The fluorescence signals may not be completely separated in tissues due to high levels of autofluorescence and low signal-to-noise ratio.[8] Additionally, when a bandpass filter around the emission maximum separates the generated emission of a fluorophore from contributions of coexcited labels, approximately 50% of the available photons are lost because they are outside the spectral range of the filter. This approach works well with standard labels, but does not work for QDs with highly overlapping spectra or unusual Stokes shifts.[9]

Molecular hyperspectral imaging (MHI) technology may offer a solution to these problems. An MHI system can collect the electromagnetic spectrum at dozens or hundreds of wavelength ranges in the spectra and produce high-dimensional spectral signature data. As shown in Fig. 1, molecular hyperspectral images record the full emission spectrum at each image pixel, which can be visualized as a three-dimensional (3-D) data cube with two spatial dimension (x, y) and a third wavelength dimension (λ). This data cube is processed using a library of reference spectra to determine the population and location of known QDs. This information allows for discrimination between different probes, as long as the spectral resolution is high enough. Therefore, MHI technology makes it possible to resolve the spectra of QD probes without switching optical filters, unmix cross-talk between overlapping fluorescence emissions, and analyze mixed contributions to a pixel.

In this letter, the water soluble CdSe and CdSe/CdS QDs are prepared and incubated with colon cancer cells for biological imaging. An MHI system is developed and used to capture both spatial and spectral data of these cells labeled with CdSe and/or CdSe/CdS QDs. A clustering algorithm is used to separate different probes and to generate coexpression and stain titer maps according to their spectral signatures to enhance the biological analysis.

The investigated CdSe and CdSe/CdS QDs are synthesized in aqueous solution under sonication by using mercaptoacetic acid (MAA) as the capping ligand. To obtain CdSe QDs, 0.1368 g of $CdCl_2 \cdot 2.5H_2O$ is dissolved in 50 mL deionized water and mixed with MAA (0.08 mL) at the pH value of 10 to 11. After a 30-min purge with N_2, 20 mL Na_2SeSO_3 solution previously prepared by the reaction of selenium with Na_2SO_3 is injected into the mixture solution while sonicating. The CdSe solution is obtained by stirring for 1 h with the molar ratio 1.5:2:1 of Cd^{2+}:MAA:Se^{2-}. To prepare the CdSe/CdS QDs, 70 mL of CdSe solution was is mixed with 100 mL of a

*Address all correspondence to: Qingli Li, E-mail: qlli@cs.ecnu.edu.cn

1083-3668/2015/$25.00 © 2015 SPIE

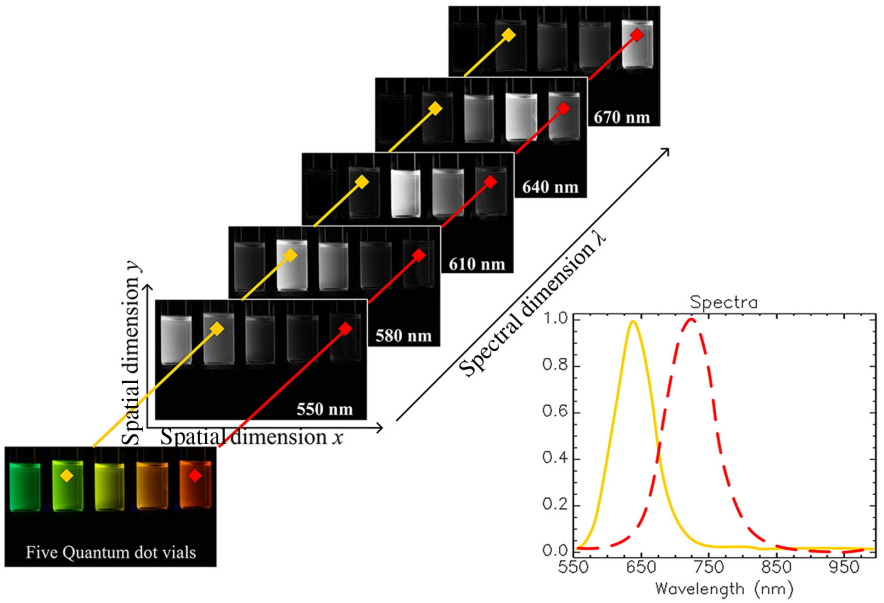

Fig. 1 Schematic diagram of three-dimensional (3-D) hyperspectral data cube and two spectra corresponding to the yellow and red pixels. Different quantum dots (QDs) can be discriminated according to their spectral signatures.

nitrogen-saturated solution containing $CdCl_2$ (1.6×10^{-3} mol) and MAA (2.13×10^{-3} mol). After stirring for 30 min, 100 mL of Na_2S (1.6×10^{-3} mol) is slowly added over a 3-h period while sonicating until the molar ratio of CdS to CdSe reaches 4:1. Finally, the CdSe/CdS nanocrystals are obtained after additional refluxing for 3 h.

To evaluate the proposed method, 500 μl of colon cancer cells (MDA-MB-231, 2×10^5/mL) is deposited onto 0.2 mm glass coverslips with 24 hole plates and incubated for 24 h. Then the substrate is extracted and 50 μl CdSe and CdSe/CdS QDs solutions are added to each hole plate and incubated for 1 h. The particle concentration is estimated by the absorbance of the particle solution according to Lambert–Beer's law.[10] After triple washing with phosphate buffered saline, the coverslips are turned upside down onto slides for observation.

Molecular hyperspectral images of labeled QDs cells are collected using a custom MHI system. As shown in Fig. 2, the system consists of a microscope, an acousto-optic tunable filter (AOTF) adapter, a fast frequency sweep (FSP) model AOTF controller, a 1/1.8 in. high-density cooled charge coupled device (CCD) detector, a data collection and control module, and a personal computer. The AOTF adapter used in this system is made from tellurium dioxide (TeO_2), which can operate as a tunable optical bandpass filter based on light–sound

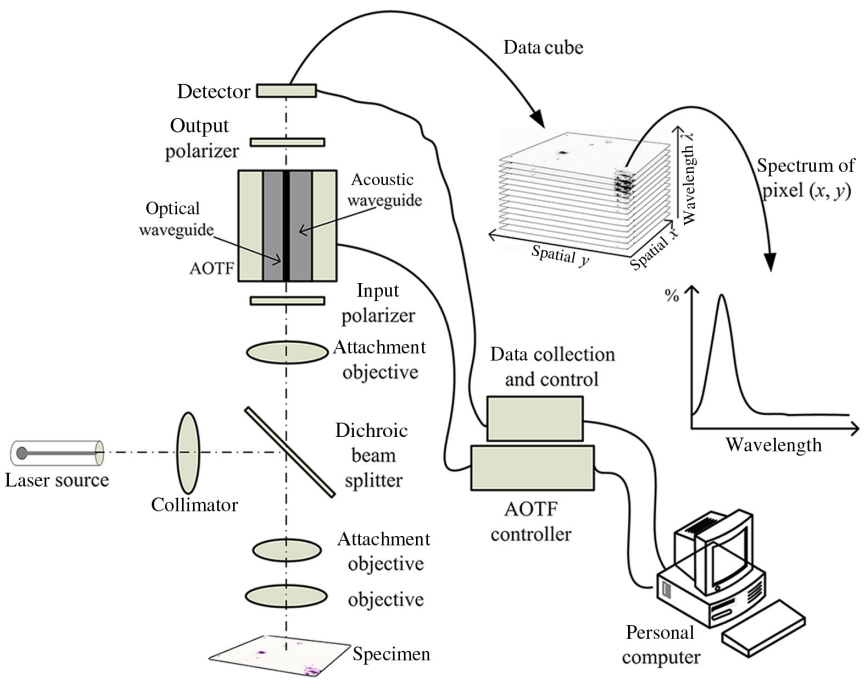

Fig. 2 Schematic diagram of the molecular hyperspectral imaging system.

interactions. The AOTF adapter is driven by a radio frequency signal generated by the FSP model controller. An acoustic wave propagating in a transparent material will produce a periodic modulation of the index of refraction. This can be regarded as a moving grating, which diffracts portions of an incident light beam.[11] With wavelength switching at the narrow bandwidth provided by the AOTF adapter, a series of single band images can be captured by the CCD detector and a 3-D data cube is obtained. The wavelength range of the MHI system is from 550 to 1000 nm and the spectral resolution is 2 to 5 nm (2 nm at 543 nm and 5 nm at 792 nm), which is suitable for multiplexed QDs' detection. The MHI system has a significant advantage over luminescence intensity imaging instruments, such as light microscopy and fluorescence microscopy, as both spatial and spectral information can be collected simultaneously.

In this study, each molecular hyperspectral image captured by the MHI system contains 60 single band images. These single band images are stored in a band sequential file format, which is optimal for spatial (x, y) access of any part of a single spectral band. Each line of the data is followed immediately by the next line in the same spectral band and the spectrum of each pixel can be extracted from the data cube and used for QD identification. Figure 3 shows the spectra of CdSe and CdSe/CdS QDs extracted from the molecular hyperspectral images captured under 400-nm excitation wavelengths. From the figure, it can be seen that the photoluminescence of CdSe/CdS QDs increased and the wavelength peak (610 nm) is red shifted 30 nm compared to CdSe QDs. As the spectral resolution of the MHI system is $\leq$5 nm, the molecular hyperspectral data can be used to properly separate two QDs from mixed labeled cells.

The molecular hyperspectral images represent the signal intensity at each pixel for the defined spectra and can be converted to composite false-color images to visualize stain distribution and intensity for each QD. Here, we use the fuzzy-C-means algorithm to separate the spectral band space into different clusters and generate false-color images. This algorithm can group pixels with similar spectra into different clusters by minimizing the sum of square errors, as shown in the following equation:

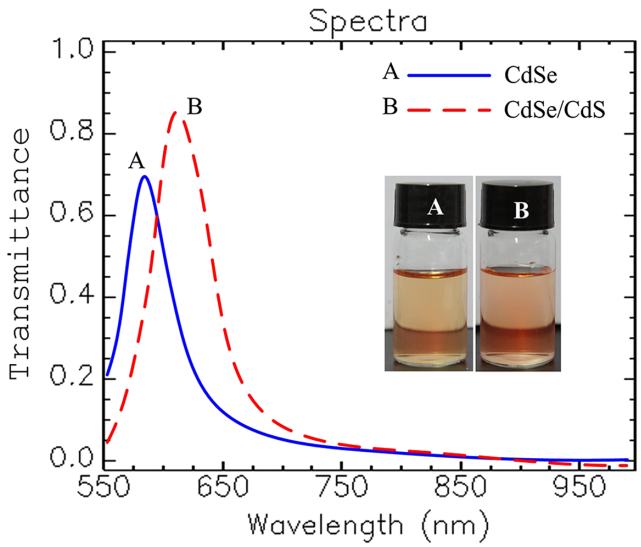

Fig. 3 Spectra of (A) CdSe QDs and (B) CdSe/CdS QDs.

$$\mathrm{SE}_{\mathrm{FCM}} = \sum_{i=1}^{c} \sum_{j=1}^{n} u_{ij}^{m} \|x_j - s_i\|^2, \tag{1}$$

where x_j denotes the spectral vector at the j'th pixel, s_i denotes the mean spectrum of fuzzy cluster i, n is the number of pixels in one band image, c is the number of clusters, and m is the weighting exponent on each fuzzy membership, which determines the amount of fuzziness of the resulting classification. The membership grade matrix $U = [u_{ij}]$ is generated for all data points and clusters. Figure 4 shows some false-color images of QD-labeled targets generated by the clustering algorithm. Figures 4(a) and 4(b) show false-color images of CdSe and CdSe/CdS labeled targets, respectively. These images show that both CdSe and CdSe/CdS QDs can be identified and visually enhanced according to their spectral signatures. Figure 4(c) shows a light microscopy image of a cell labeled with CdSe and CdSe/CdS QDs, and Fig. 4(d) shows the coexpression false-color image of the same cell synthesized by the identification results and single band images extracted from the molecular hyperspectral images as the red (R), green (G), and blue (B) channels, respectively. From Figs. 4(c) and 4(d), it can be seen that the traditional light microscopy method can barely distinguish the two QDs, as most of their spectra overlap, whereas the hyperspectral-based method produces enhanced visualizations of different QDs in multilabeled targets. Figure 4(d) also indicates that CdSe and CdSe/CdS QDs can enter tumor cells efficiently, which can be used for live cells imaging. In addition, the stain titer maps of QDs can be calculated and represented by virtual 3-D images created by data fusion, which is capable of integrating different imagery data and creating more information than can be derived from a light microscopy image. Figure 5 shows a 3-D representation of CdSe stain titer at two different viewing angles. This data was generated by integrating the high spatial and spectral resolutions provided by molecular hyperspectral data and the false-color images. These fused virtual

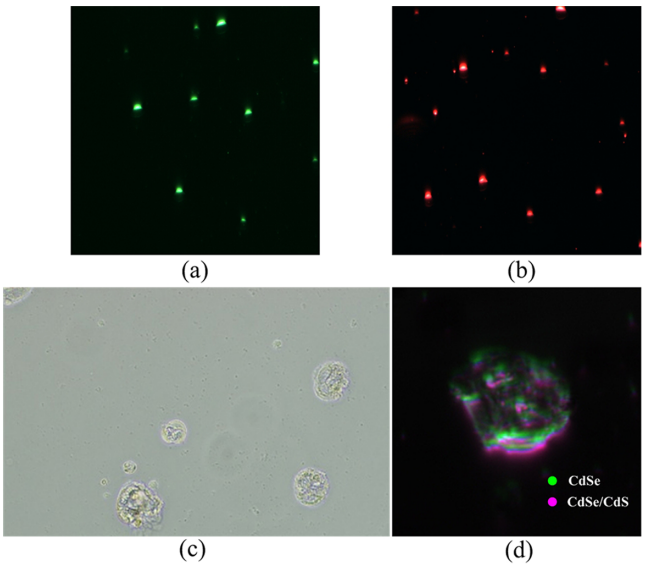

Fig. 4 Images of QDs labeled targets and coexpression results. (a and b) False-color images of CdSe and CdSe/CdS QDs labeled targets, respectively, (c) light microscopy image (bright field) of a multilabeled cell by the two QDs, (d) coexpression false-color image synthesized by the identification results and single band images extracted from the molecular hyperspectral images.

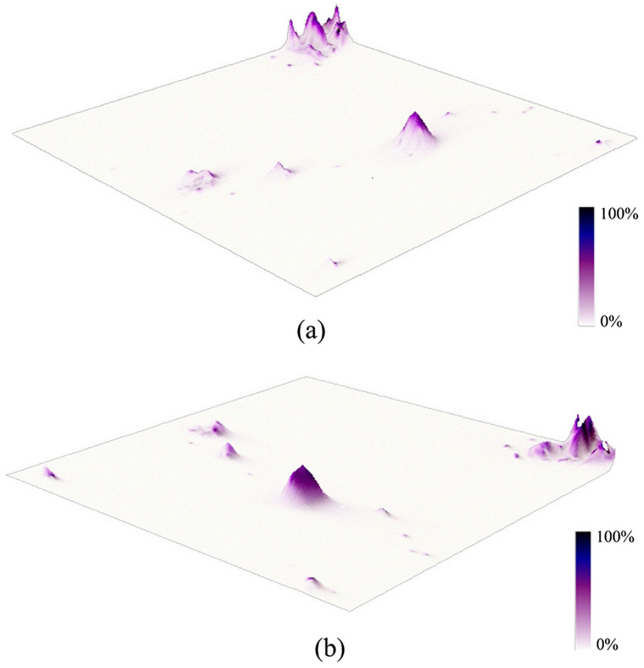

Fig. 5 Virtual 3-D view of one scene image from (a) angle and (b) angle.

Table 1 Dependence of death ratio (%) for Caco-2 cell line on the concentration of CdSe or CdSe/CdS quantum dots by 3-(4,5)-dimethylthiahiazo (-z-y1)-3,5-di-phenytetrazoliumromide viability assay.

Concentration (mmol/L)	60	100	160	200
CdSe	2.5 ± 0.1	9.3 ± 0.4	12.6 ± 0.5	15.8 ± 0.5
CdSe/CdS	18.8 ± 0.6	42.9 ± 0.8	43.3 ± 0.8	44.7 ± 0.7

3-D images can provide a stain titer view of QDs, which are useful for biological analysis. It is noteworthy that the cytotoxicity of CdSe and CdSe/CdS QDs can be higher than that of standard fluorophores, which will result in some cell death before observation. To evaluate the cytotoxicity of QDs, 3-(4,5)-dimethylthiahiazo (-z-y1)-3,5-di-phenytetrazoliumromide (MTT) viability assay was conducted on a Caco-2 cell line. Table 1 lists the experimental results, which show that if the concentration of the QDs is under 60 mmol/L, 80% of the Caco-2 cells will survive for observation. We will further investigate the influence of cytotoxicity of CdSe and CdSe/CdS QDs in future studies.

In this letter, MHI of CdSe or/and CdSe/CdS QD-labeled cells is reported. The hyperspectral-based method allows for direct experimental investigation of the fluorescence properties of different QDs over the 550 to 1000 nm spectral range with a 50 nm spectral resolution. By using the spectral difference of CdSe and CdSe/CdS QDs emission and a clustering algorithm, the enhanced visualization and coexpression of multilabeled cells can be realized. These results demonstrate that the custom MHI system provides a potential tool for multibiomarkers' recognition from the visible to the near-infrared spectrum at the cellular level.

Acknowledgments

This work was supported in part by the National Natural Science Foundation of China (Grant Nos. 61177011 and 61377107), the Science and Technology Commission of Shanghai Municipality (Grant No. 14DZ2260800), and the project supported by the State Key Development Program for Basic Research of China (Grant No. 2011CB932903).

References

1. K. D. Wegner and N. Hildebrandt, "Quantum dots: bright and versatile in vitro and in vivo fluorescence imaging biosensors," *Chem. Soc. Rev.* **44**(14), 4792–4834 (2015).
2. O. Halder et al., "Highly luminescent two dimensional excitons in atomically thin CdSe nanosheets," *Appl. Phys. Lett.* **104**(18), 182109 (2014).
3. M. Adeli et al., "Quantum dot-pseudopolyrotaxane supramolecules as anticancer drug delivery systems," *Polymer* **52**(11), 2401–2413 (2011).
4. X. Ji et al., "Fluorescent quantum dots: synthesis, biomedical optical imaging, and biosafety assessment," *Colloids Surf. B* **124**(12), 132–139 (2014).
5. X. Chen et al., "Microwave-assisted synthesis of glutathione-capped CdTe/CdSe near-infrared quantum dots for cell imaging," *Int. J. Mol. Sci.* **16**(5), 11500–11508 (2015).
6. C. Yanlin et al., "Ultrasensitive fluorescence detection of heparin based on quantum dots and a functional ruthenium polypyridyl complex," *Biosens. Bioelectron.* **55**(5), 174–179 (2014).
7. M. Fang et al., "Quantum dots-based in situ molecular imaging of dynamic changes of collagen IV during cancer invasion," *Biomaterials* **34**(34), 8708–8717 (2013).
8. S. J. Leavesley et al., "Hyperspectral imaging microscopy for identification and quantitative analysis of fluorescently-labeled cells in highly autofluorescent tissue," *J. Biophotonics* **5**(1), 67–84 (2012).
9. T. Zimmermann, "Spectral imaging and linear unmixing in light microscopy," in *Microscopy Techniques*, J. Rietdorf, Ed., pp. 245–265, Springer-Verlag, Berlin Heidelberg (2005).
10. W. W. Yu et al., "Experimental determination of the extinction coefficient of CdTe, CdSe, and CdS nanocrystals," *Chem. Mater.* **15**(14), 2854–2860 (2003).
11. C. D. Tran, "Acousto-optic tunable filter: a new generation onochromator and more," *Anal. Lett.* **33**(9), 1711–1732 (2000).